

Supporting Information

For

Oxygen Transfer in Electrophilic Epoxidation Probed by ^{17}O NMR: Differentiating Between Oxidants and Role of Spectator Metal Oxo

Christian Ehinger,[‡] Christopher P. Gordon,[‡] Christophe Copéret*

Department of Chemistry and Applied Biosciences, ETH Zürich, Vladimir Prelog Weg 1-5, 8093, Zürich, Switzerland.

Contents:

1. Computational Details	S2
2. Calculations of Shielding Tensors	S3
3. Quadrupolar Coupling Calculations of MTO, Bis- and Monoperoxide	S5
4. Chemical Shielding Tensor Orientations in MTO peroxy species	S6
5. Graphical Representation of the Results of the NCS Analysis	S7
6. Visual Representations of Relevant NLMOs of Peroxide Compounds	S10
7. Graphical Representation of the Calculated EFG Tensors	S11
8. Natural Hybrid Orbital (NHO) Directionality and Bond Bending Analysis	S12
9. Experimental Section	S13
10. Solid-State NMR Spectra and Simulations	S13
11. Optimized Structures of all Calculated Species	S14
12. References	S15

1. Computational Details

All geometry optimizations were performed with the Gaussian09 package^[1] at the PBE0 level.^[2] Re was represented by a quasi-relativistic core potential (RECP) from the Stuttgart group and the associated basis set^{[3]-[5]}. The remaining atoms (H, C, N, O and Cl) were represented by a triple- ζ pcseg-2 basis set.^[6] NMR calculations were performed within the GIAO framework using ADF 2014^[7] with the PBE0 functional and Slater-type basis sets of triple- ζ quality (TZ2P). Relativistic effects were treated by the 2 component zeroth order regular approximation (ZORA).^{[8]-[12]} Analysis of scalar-relativistic natural localized molecular orbitals were done with the NBO 6.0 program.^[13] Calculated NMR shielding tensors were analyzed using these scalar-relativistic NLMOs.^{[14]-[17]} The 3D representation of the calculated shielding tensors is obtained as polar plots^{[18],[19]} of functions $\sum_{ij} r_i \sigma_{ij} r_j$, with scaling factors adjusted towards the best readability.

EFG tensors were calculated using the ADF 2014 code, using the PBE0 functional and a Slater-type TZ2P basis set on all atoms.

Energies were calculated as single point calculations from the optimized structures, using GD3 dispersion corrections^[20] and the SMD model^[21] to account for the solvent (dichloromethane).

2. Calculations of Shielding Tensors

Table S1: ^{17}O shielding- and chemical shift tensor principle components of investigated peroxides and non-peroxide analogues (all values in ppm).

Compound	σ_{11}	σ_{22}	σ_{33}	σ_{iso}	δ_{11}	δ_{22}	δ_{33}	δ_{iso}
H ₂ O	310	327	367	335	25	8	-32	0
H ₂ O ₂	-30	108	342	140	364	227	-7	195
DMDO	-301	171	262	44	636	164	73	291
Acetone	-904	-405	312	-332	1239	740	23	667
mCPBA (OH)	-205	89	285	56	540	245	50	278
mCPBA (O)	-93	74	99	27	428	261	236	308
mCBA (OH)	-7	174	259	142	342	161	76	193
mCBA (C=O)	-283	-200	293	-63	618	535	42	398
tBuOOH (O)	-78	0	262	61	413	335	73	273
tBuOOH (OH)	-51	107	333	130	386	228	2	205
tBuOH	205	231	283	240	130	104	52	95
MeReO ₂ (O ₂)Py <i>trans</i>	-361	-22	114	-90	695	357	221	425
MeReO ₂ (O ₂)Py <i>cis</i>	-230	-45	23	-84	565	380	312	419
MeReO(O ₂) ₂ Py <i>trans</i>	-193	-71	134	-43	528	406	201	378
MeReO(O ₂) ₂ Py <i>cis</i>	-228	-23	9	-81	563	358	326	416
MeReO(O ₂) ₂ OH ₂ <i>trans</i>	-172	-59	143	-29	507	394	192	364
MeReO(O ₂) ₂ OH ₂ <i>cis</i>	-237	-30	6	-87	572	365	329	422
MeReO ₂ (O ₂) <i>trans</i>	-311	0	100	-70	646	335	235	405
MeReO ₂ (O ₂) <i>cis</i>	-267	-39	-1	-102	602	374	336	437
MTO	-1058	-383	-236	-559	1392	718	571	894

Table S2: NCS analysis of investigated peroxides – σ_{11} (all values in ppm).

	σ_{para}	σ_{dia}	LP 'p'	LP 's'	components of σ_{para}	
					$\sigma(\text{R-O/Re-O})$	$\sigma(\text{O-O})$
H ₂ O ₂	-412	379	-415	-7	-4	7
tBuOOH (O)	-472	380	-462	-5	0	-16
tBuOOH (OH)	-434	382	-427	-18	-10	18
mCPBA (O)	-491	381	-175	-35	-175	-37
mCPBA(OH)	-584	382	-561	-	-	-15
DMDO	-692	388	-699	-	-	-
MeReO(O ₂) ₂ Py <i>cis</i>	-613	390	-411	-9	-127	-37
MeReO(O ₂) ₂ Py <i>trans</i>	-575	386	-424	-	-126	-33
MeReO ₂ (O ₂)Py <i>cis</i>	-616	386	-518	-10	-34	-56
MeReO ₂ (O ₂)Py <i>trans</i>	-751	389	-421	-29	-288	-25
MeReO(O ₂) ₂ OH ₂ <i>cis</i>	-612	387	-406	-	-172	-43
MeReO(O ₂) ₂ OH ₂ <i>trans</i>	-558	387	-399	-	-118	-42
MeReO ₂ (O ₂) <i>cis</i>	-650	383	-523	-	-54	-65
MeReO ₂ (O ₂) <i>trans</i>	-697	386	-405	-14	-264	-33

Table S3: NCS analysis of investigated peroxides – σ_{22} (all values in ppm).

	σ_{para}	σ_{dia}	LP 'p'	LP 's'	components of σ_{para}	
					$\sigma(\text{R-O/Re-O})$	$\sigma(\text{O-O})$
H2O2	-256	361	-5	-80	-153	-23
tBuOOH (O)	-358	362	0	-154	-144	-37
tBuOOH (OH)	-259	362	-11	-62	-165	-24
mCPBA (O)	-289	361	-	-101	-78	-80
mCPBA(OH)	-271	364	-	-86	-202	13
DMDO	-190	361	2	-66	-197	96
MeReO(O2)2Py <i>cis</i>	-409	385	-313	-39	-59	-12
MeReO(O2)2Py <i>trans</i>	-454	382	-261	-46	-109	-17
MeReO2(O2)Py <i>cis</i>	-435	392	-258	-31	-172	8
MeReO2(O2)Py <i>trans</i>	-406	380	-229	-44	-85	-29
MeReO(O2)2 OH2 <i>cis</i>	-413	380	-231	-40	-170	11
MeReO(O2)2 OH2 <i>trans</i>	-437	382	-271	-37	-144	0
MeReO2(O2) <i>cis</i>	-425	386	-260	-17	-188	6
MeReO2(O2) <i>trans</i>	-382	382	-257	-33	-43	-43

Table S4: NCS analysis of investigated peroxides – σ_{33} (all values in ppm).

	σ_{para}	σ_{dia}	LP 'p'	LP 's'	components of σ_{para}	
					$\sigma(\text{R-O/Re-O})$	$\sigma(\text{O-O})$
H2O2	-59	394	-56	7	1	-13
tBuOOH (O)	-143	399	-110	-10	4	-
tBuOOH (OH)	-70	393	-47	-6	-16	0
mCPBA (O)	-300	388	-150	-81	-11	-64
mCPBA(OH)	-118	393	-67	-7	-35	-
DMDO	-130	388	-109	-	10	-9
MeReO(O2)2Py <i>cis</i>	-347	366	-22	-66	-244	-17
MeReO(O2)2Py <i>trans</i>	-232	364	-35	-29	-144	0
MeReO2(O2)Py <i>cis</i>	-336	365	-3	-61	-341	105
MeReO2(O2)Py <i>trans</i>	-255	366	-26	-28	-228	55
MeReO(O2)2 OH2 <i>cis</i>	-356	367	-79	-66	-268	73
MeReO(O2)2 OH2 <i>trans</i>	-222	365	-28	-28	-264	114
MeReO2(O2) <i>cis</i>	-362	360	10	-62	-357	102
MeReO2(O2) <i>trans</i>	-259	359	9	-28	-299	103

3. Quadrupolar Coupling Calculations MTO, -Bisperoxide and -Monoperoxide

Table S5: C_Q Parameters of MTO-derived compounds

	C_Q [MHz]	V_{33} [a.u.]	η_Q
MTO	-4.58	0.76	0.56
MeReO(O2)2Py <i>oxo</i>	2.14	-0.36	0.10
MeReO(O2)2Py <i>trans</i>	-15.16	2.52	0.92
MeReO(O2)2Py <i>cis</i>	-14.97	2.49	0.85
MeReO2(O2)Py <i>oxo 1</i>	-5.06	0.84	0.32
MeReO2(O2)Py <i>oxo 2</i>	-5.07	0.84	0.94
MeReO2(O2)Py <i>trans</i>	-13.00	2.16	0.91
MeReO2(O2)Py <i>cis</i>	-17.21	2.86	0.70
MeReO(O2)2 OH2 <i>oxo</i>	1.34	-0.22	0.32
MeReO(O2)2 OH2 <i>trans</i>	-14.98	2.49	0.95
MeReO(O2)2 OH2 <i>cis</i>	-14.98	2.49	0.89
MeReO2(O2) <i>oxo 1</i>	-4.53	0.75	0.76
MeReO2(O2) <i>oxo 2</i>	-4.53	0.75	0.76
MeReO2(O2) <i>trans</i>	-13.27	2.21	0.94
MeReO2(O2) <i>cis</i>	-16.21	2.70	0.81

4. Chemical Shielding Tensor Orientations in MTO peroxy species

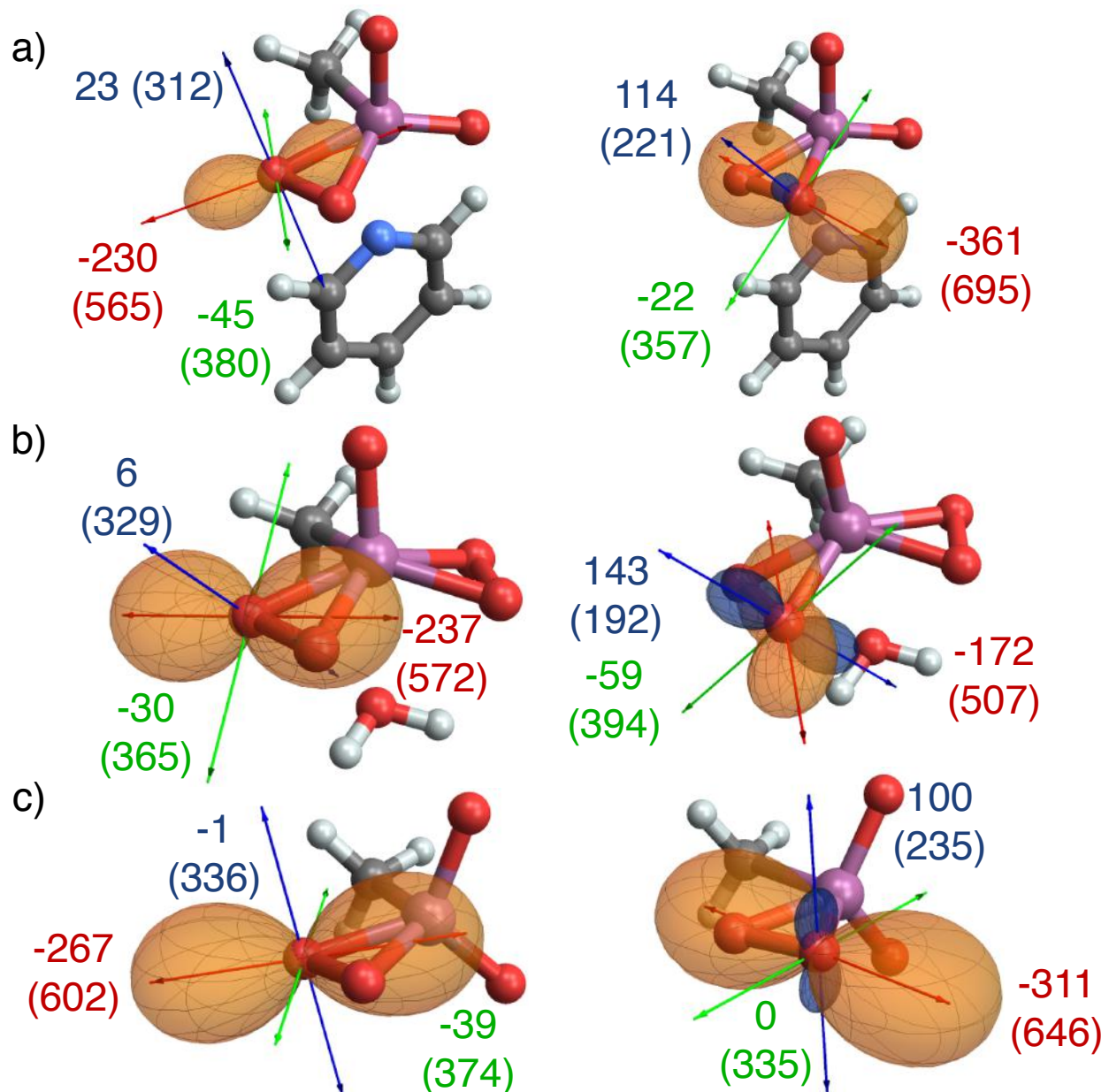


Figure S1. CST Orientation for the peroxy oxygens a) $\text{MeReO}_2(\text{O}_2)\text{Py}$, b) $\text{MeReO}(\text{O}_2)_2 \text{OH}_2$ and c) $\text{MeReO}_2(\text{O}_2)$. Shielding values (σ) are shown in ppm, with the corresponding chemical shift values (δ) in parenthesis.

5. Graphical Representation of the Results of the NCS Analysis

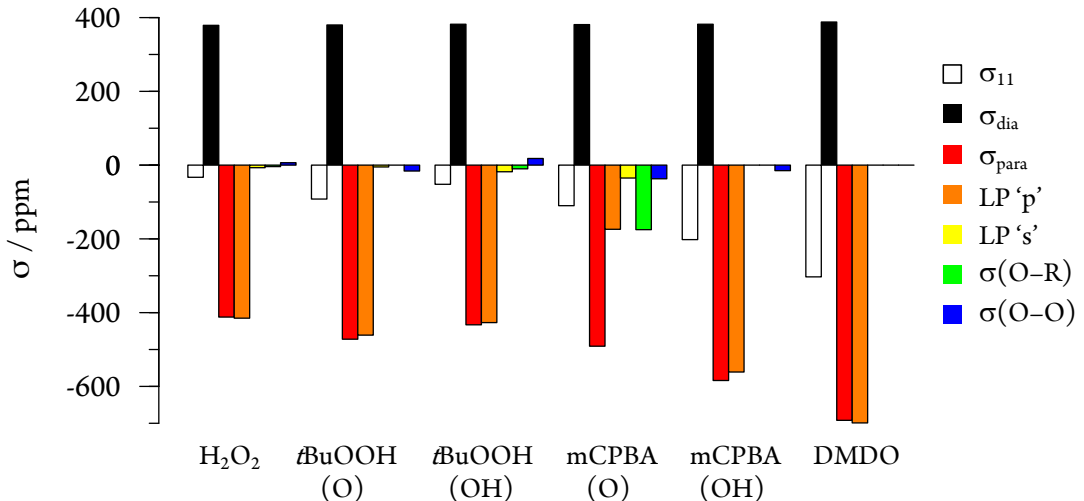


Figure S2. Non-metal-based peroxides – σ_{11} components (reproduction of Figure 4b in main text).

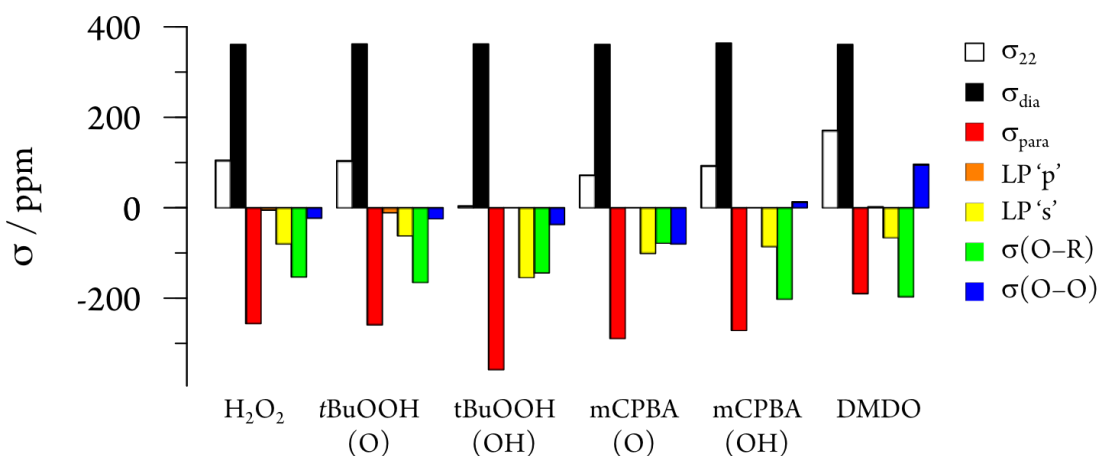


Figure S3. Non-metal-based peroxides – σ_{22} components. The dominant contributions arise from the $\sigma(O-R)$ and LP 's', judging from the tensor orientation both orbitals couple to $\sigma^*(O-O)$. $\sigma(O-O)$ also contributes in all cases, for mCPBA (OH) and DMDO its contribution is shielding.

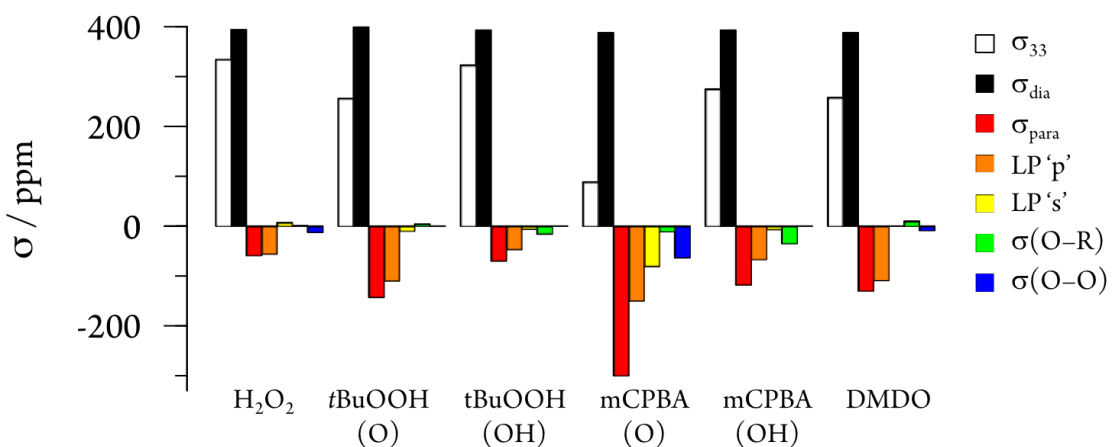


Figure S4. Non-metal-based peroxides – σ_{33} components.

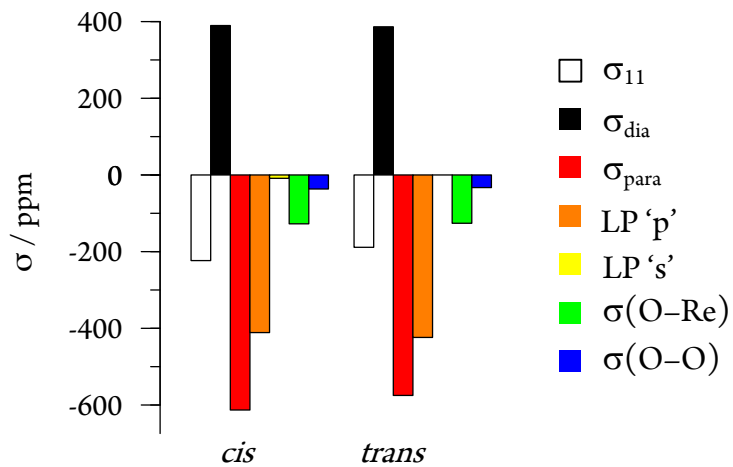


Figure S5. MTO bisperoxide – σ_{11} components (reproduction of Figure 9b in main text).

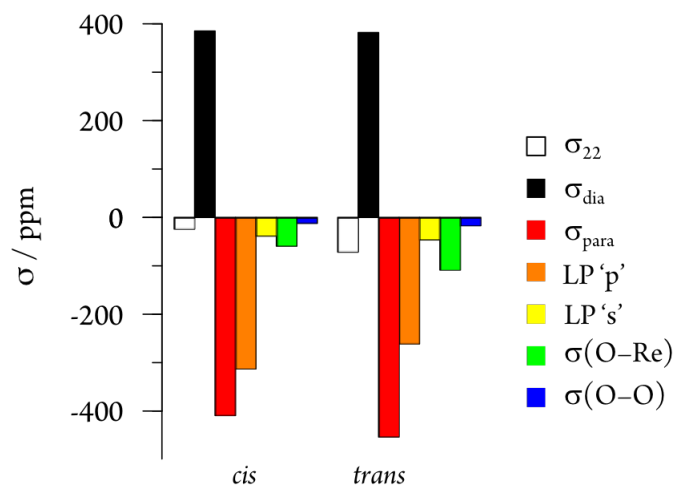


Figure S6. MTO bisperoxide – σ_{22} components. The dominant contribution arises from the LP 'p'.

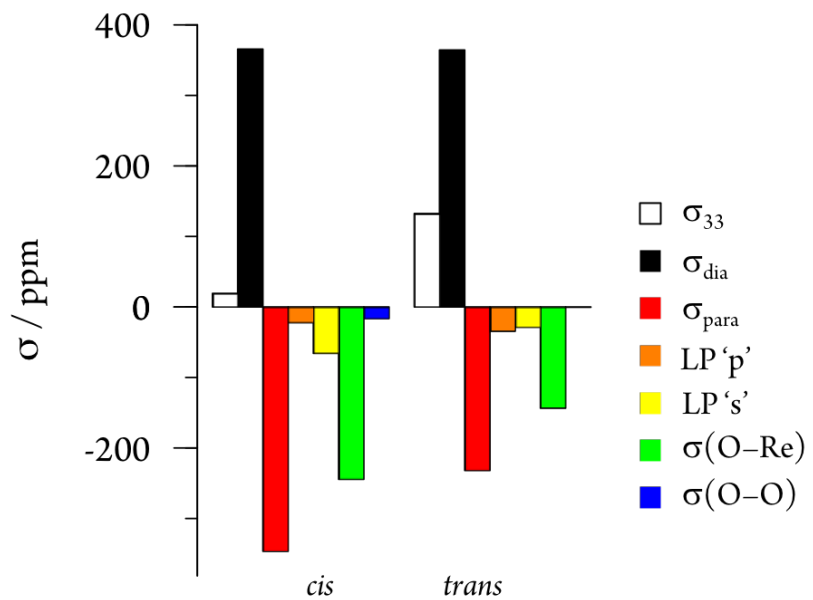


Figure S7. MTO bisperoxide – σ_{33} components. The dominant contribution to deshielding arises from $\sigma(O-Re)$ which presumably couples to $\sigma^*(O-O)$.

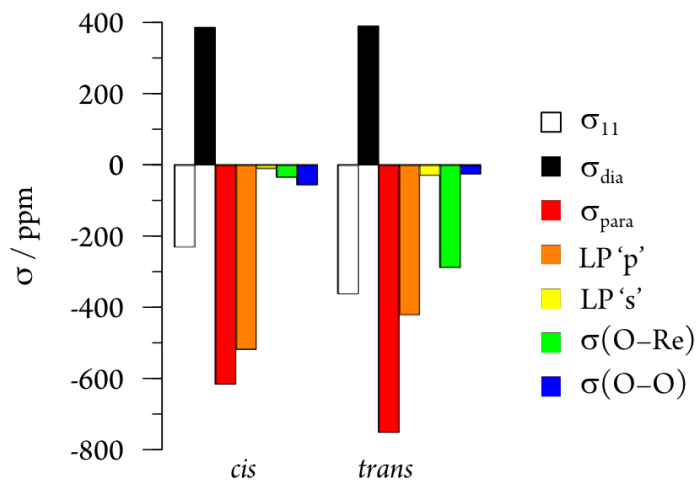


Figure S8. MTO monoperoxide – σ_{11} components. For the *cis* oxygen, the contribution of the LP ‘p’ is dominating, for the *trans* oxygen, $\sigma(O-Re)$ also contributes significantly.

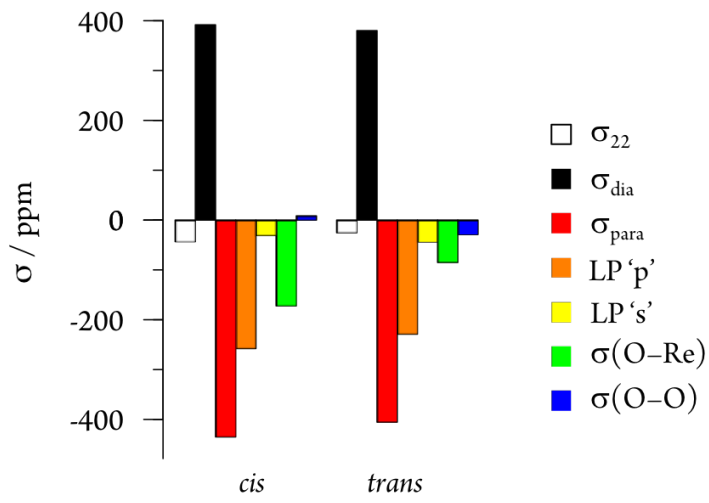


Figure S9. MTO monoperoxide – σ_{22} components. For both the *cis* and the *trans* oxygen, LP ‘p’ and $\sigma(O-Re)$ contributions to σ_{para} are the most significant.

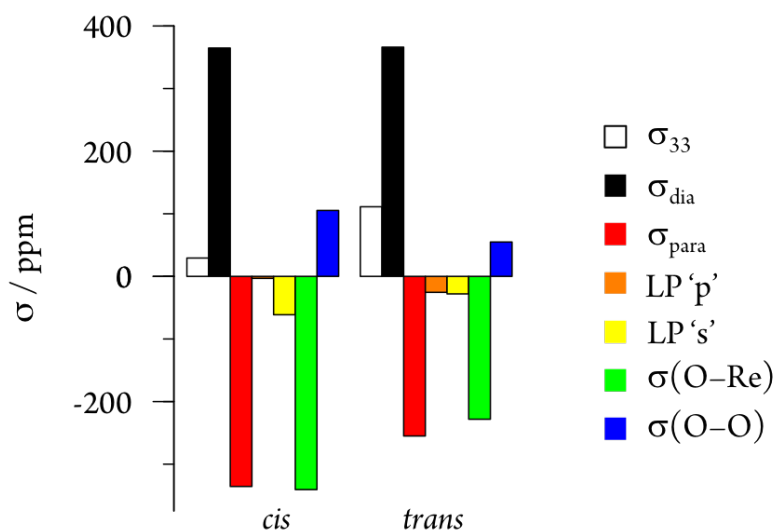


Figure S10. MTO monoperoxide – σ_{33} components. The largest deshielding arises from $\sigma(O-Re)$; similar to the DMDO and mCPBA (OH) σ_{22} -component, $\sigma(O-O)$ contributes to shielding of σ_{para} .

6. Visual Representations of Relevant NLMOs of Peroxide Compounds

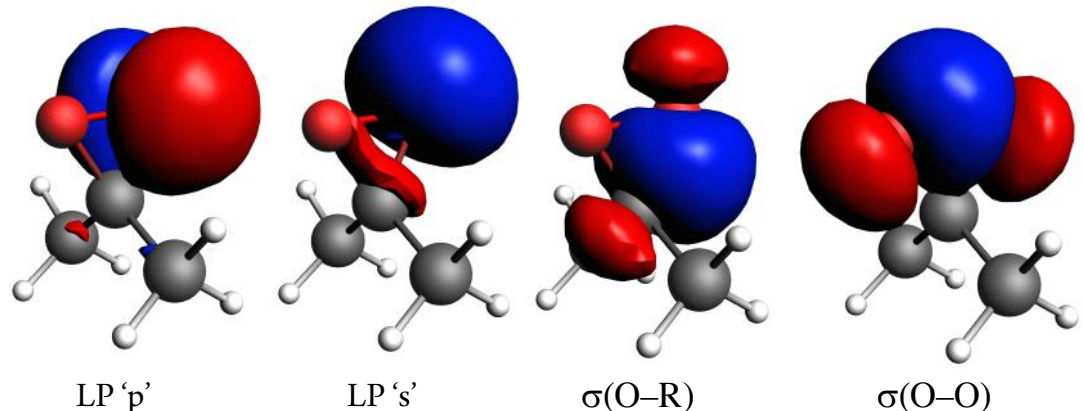


Figure S11. NLMOs of DMDO with relevance to the paramagnetic deshielding.

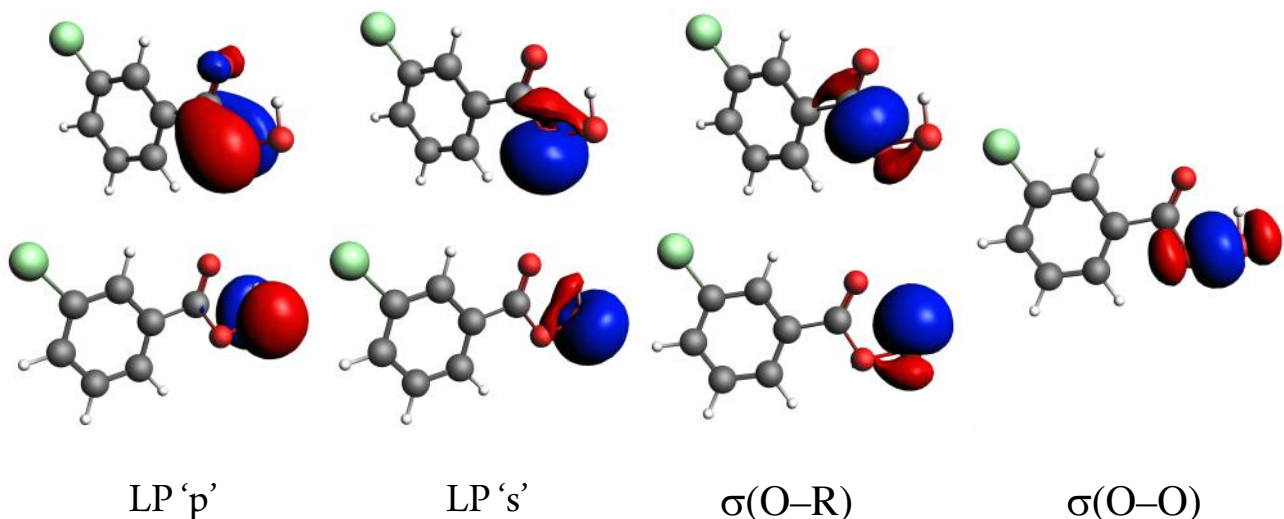


Figure S12. NLMOs of mCPBA with relevance to the paramagnetic deshielding.

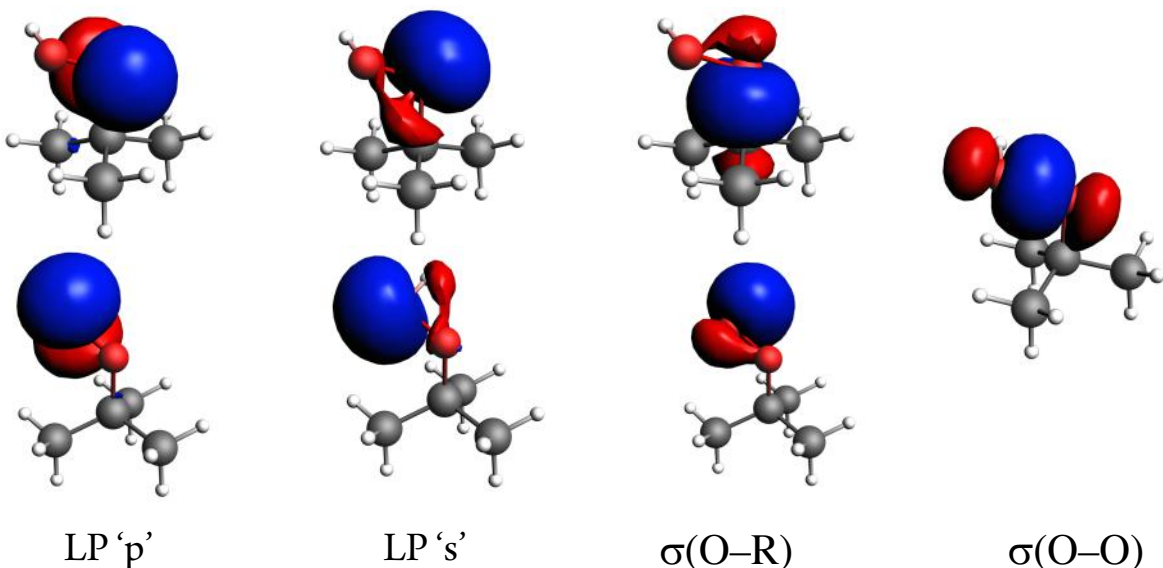


Figure S13. NLMOs of *t*BuOOH with relevance to the paramagnetic deshielding.

7. Graphical Representation of the Calculated EFG Tensors

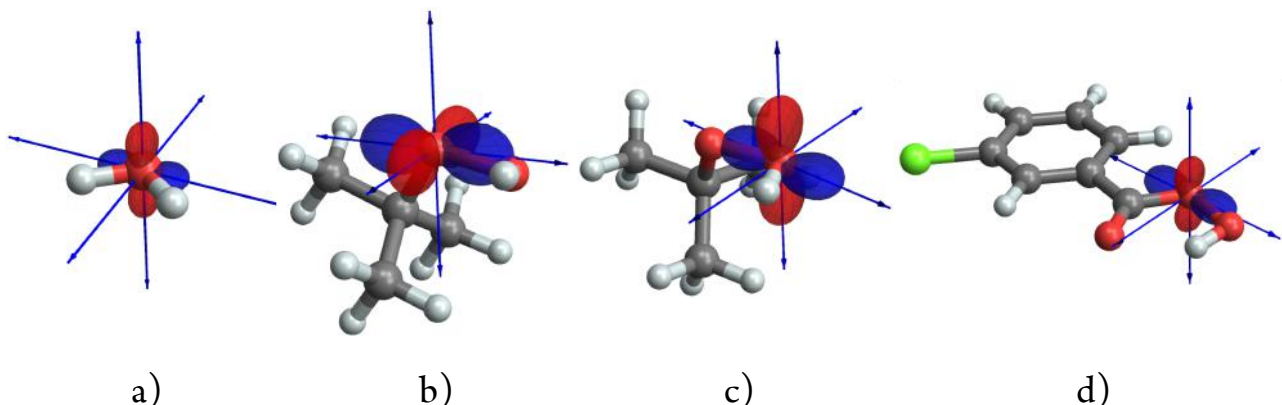


Figure S14. Representation of ^{17}O EFG tensors of a) H_2O , b) $t\text{BuOOH}$ (O), c) $t\text{BuOOH}$ (OH) and d) mCPBA (O).

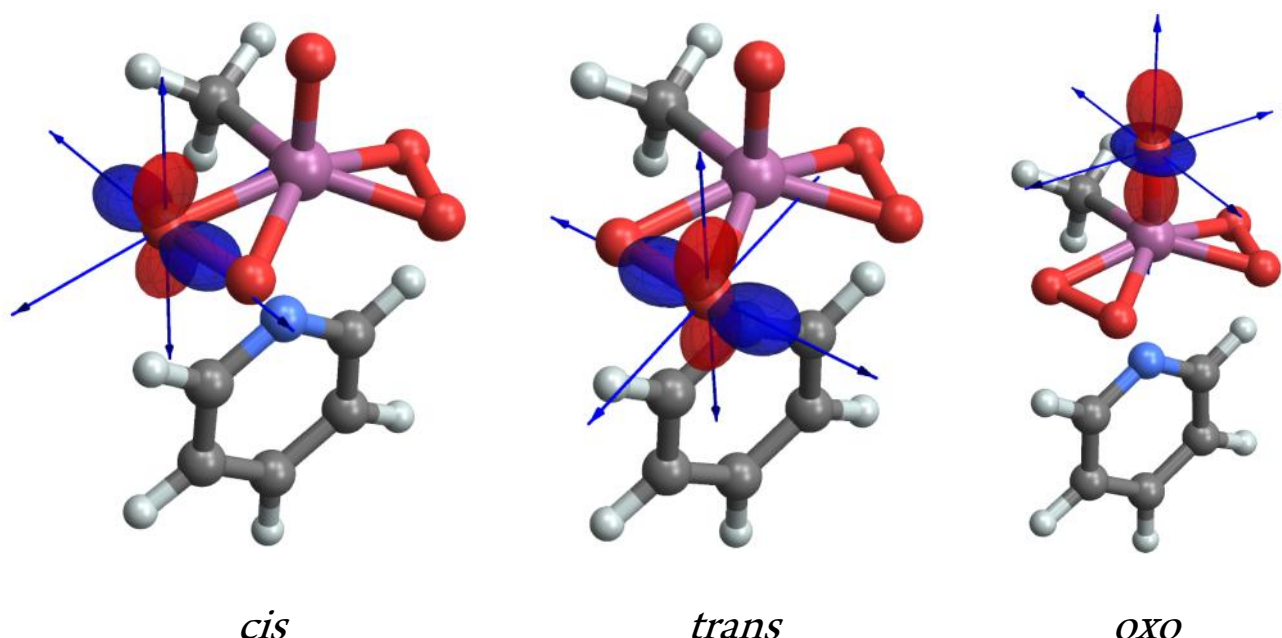


Figure S15. Representation of ^{17}O EFG tensors of the MTO bisperoxide of the peroxy-oxygens pseudo-*cis* and pseudo-*trans* to the methyl group (*cis*: $C_Q = -15.0$ MHz, $\eta = 0.85$; *trans*: $C_Q = -15.2$ MHz, $\eta = 0.92$; *oxo*: $C_Q = 2.14$ MHz, $\eta = 0.10$). The size of the EFG tensor for the oxo-oxygen is increased by a factor of eight with respect to the peroxy-oxygen atoms.

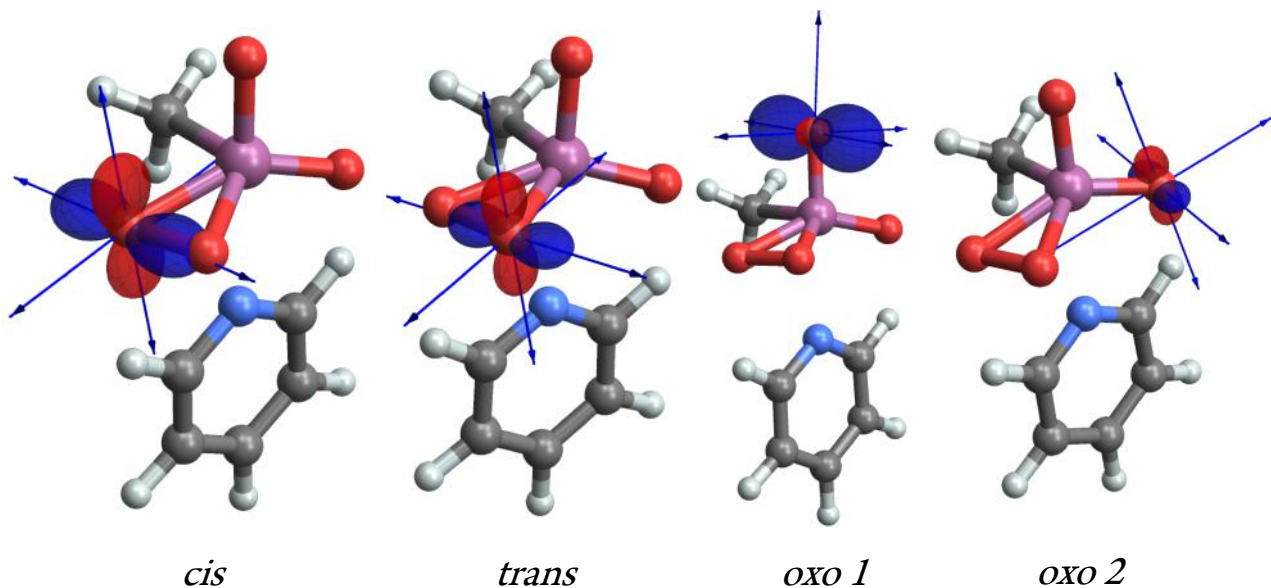


Figure S16. Representation of ^{17}O EFG tensors of the MTO monoperoxide of the peroxy-oxygens pseudo-*cis* and pseudo-*trans* to the methyl group (cis: $C_Q = -13.0$ MHz, $\eta = 0.91$; trans: $C_Q = -17.2$ MHz, $\eta = 0.70$, oxo 1: $C_Q = -5.06$ MHz, $\eta = 0.32$; oxo 2: $C_Q = -5.08$ MHz, $\eta = 0.94$). The size of the EFG tensor for the oxo-oxygen atoms is increased by a factor of two with respect to the peroxy-oxygen atoms.

8. Natural Hybrid Orbital (NHO) Directionality and Bond Bending Analysis

Table S6: Deviation of the natural hybrid orbitals from the O–O axis.

	NHO deviation
H_2O_2	2.5°
$t\text{BuOOH}$	1.9°
$m\text{CPBA}$	2.8°
DMDO	16.8°
$\text{MeReO}(\text{O}_2)_2\text{L}$	2.5°
$\text{MeReO}_2(\text{O}_2)\text{L}$	9.5°

9. Experimental Section

NMR Measurements

All measurements were obtained on a Bruker Avance III 600 MHz NMR spectrometer (14.1 T) at low temperatures (110 K) using a 3.2 mm probe. The magnetic field was externally referenced by setting the signal of liquid H₂O (at RT) to 0 ppm. Measurements were performed in a 3.2 mm zirconia rotor closed with a VESPEL drive cap, or in a 3.2 mm sapphire rotor closed with a zirconia cap. Static WURST-CPMG^[22] (Wideband, Uniform Rate, and Smooth Truncation pulse with CPMG echo-train acquisition) experiments were performed to obtain the ¹⁷O NMR spectra. Detail of the WURST pulse: 50 us length, 80 steps, 0.5 MHz sweep width, sweeping from low to high frequency. SPINAL64 with 100 kHz rf-frequency was used for ¹H decoupling. Simulations of the spectra were performed using the QUEST software.^[23]

Synthesis of ¹⁷O labelled compounds and sample preparation

¹⁷O enriched H₂O₂ was synthesized according to literature procedure^[24] and impregnated on mesoporous silica prior to measurement (ca. 1 μ l of 1.4 wt% aqueous solution per mg of solid).

¹⁷O enriched acetone was synthesized according to literature procedure^[25] using H₂¹⁷O in place of H₂¹⁸O. The sample was measured as a frozen solution.

¹⁷O enriched MTO was synthesized according to literature procedure.^[26]

10. Solid-State NMR Spectra and Simulations

For the molecules considered in this study, both the chemical shift anisotropy (CSA) and the quadrupolar coupling significantly impact the appearance of the ¹⁷O NMR spectrum. Hence, the simulation of the spectra depends on 8 parameters: 3 for the CSA (the isotropic chemical shift δ_{iso} , the span Ω and the skew κ , or alternatively the three principal components of the chemical shift tensor δ_{11} , δ_{22} , and δ_{33}), 2 for the quadrupolar interaction (C_Q and η), and 3 parameters relating the orientation of the chemical shift tensor to the orientation of the EFG-tensor (Euler angles α , β , and γ). The simulation of one spectrum with 8 independent parameters is associated with a significant uncertainty associated with each of the parameters. Herein the spectra were simulated starting with information obtained from DFT calculations as a first guess, and then modifying the individual parameters until a good simulation of the experimental spectrum was obtained. While the obtained simulated spectra hence provide a benchmark for the calculated values, showing that the results obtained from DFT calculations are at least reasonable, the exact numbers should be considered with caution.

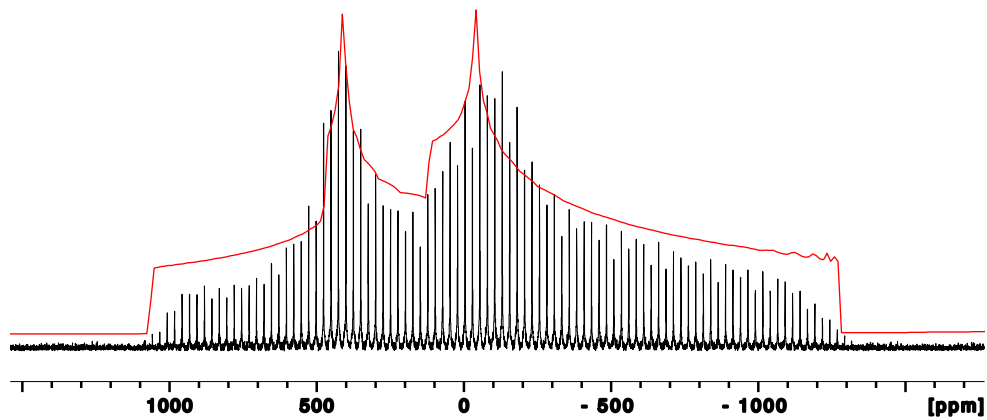


Figure S17. WURST-CPMG spectrum (black) of H_2O_2 and corresponding simulation (red). Simulation parameters: $C_Q = -16 \text{ MHz}$, $\eta = 0.8$, $\delta_{\text{iso}} = 195 \text{ ppm}$, $\Omega = 370 \text{ ppm}$, $\kappa = 0.3$, $\alpha = \beta = \gamma = 0^\circ$.

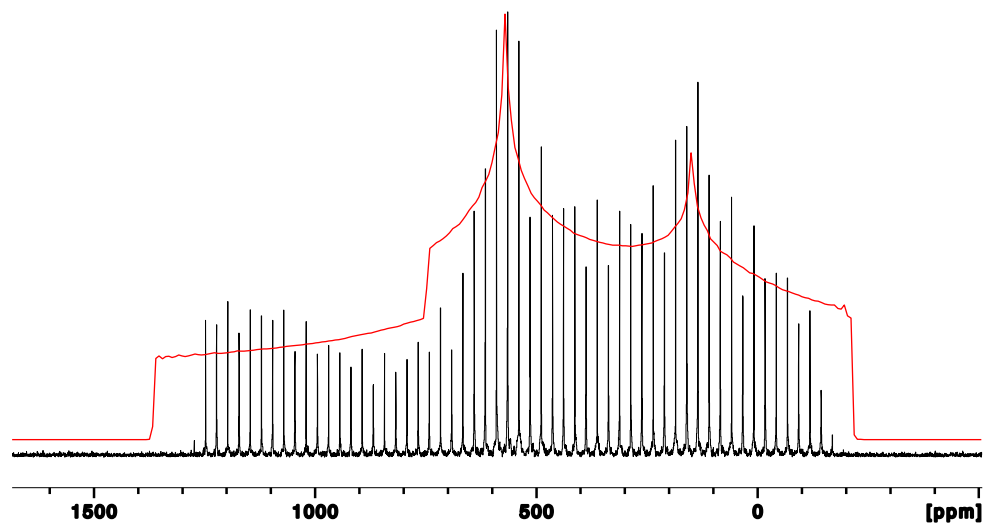


Figure S18. WURST-CPMG spectrum (black) of acetone and corresponding simulation (red). Simulation parameters: $C_Q = 12 \text{ MHz}$, $\eta = 0.6$, $\delta_{\text{iso}} = 625 \text{ ppm}$, $\Omega = 1200 \text{ ppm}$, $\kappa = 0.2$, $\alpha = 45^\circ$, $\beta = \gamma = 90^\circ$.

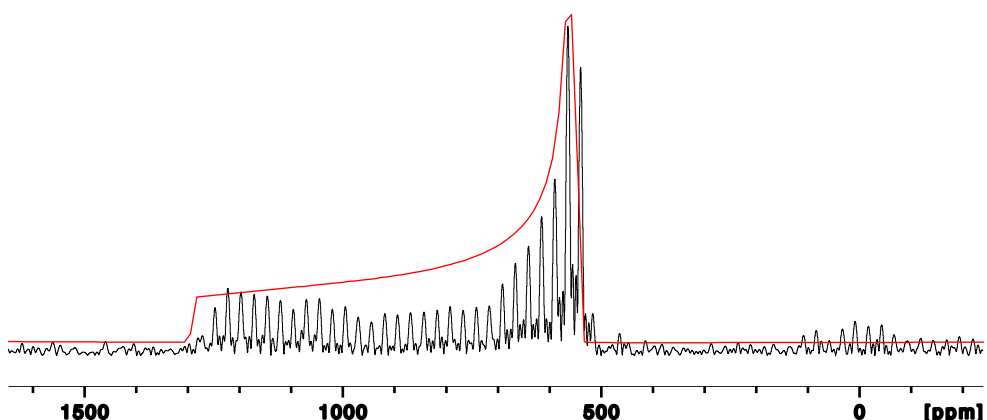


Figure S19. WURST-CPMG spectrum (black) of MTO and corresponding simulation (red). Simulation parameters: $C_Q = -4 \text{ MHz}$, $\eta = 0.6$, $\delta_{\text{iso}} = 820 \text{ ppm}$, $\Omega = 820 \text{ ppm}$, $\kappa = -0.7$, $\alpha = 0^\circ$, $\beta = 90^\circ$, $\gamma = 60^\circ$.

11. Optimized Structures of all Calculated Species

Optimized Structures of all species are provided as .xyz files as supplementary material.

12. References

- [1] Frisch, M. J.; Trucks, G. W.; Schlegel, H. B.; Scuseria, G. E.; Robb, M. A.; Cheeseman, J. R.; Scalmani, G.; Barone, V.; Mennucci, B.; Petersson, G. A.; Nakatsuji, H.; Caricato, M.; Li, X.; Hratchian, H. P.; Izmaylov, A. F.; Bloino, J.; Zheng, G.; Sonnenberg, J. L.; Hada, M.; Ehara, M.; Toyota, K.; Fukuda, R.; Hasegawa, J.; Ishida, M.; Nakajima, T.; Honda, Y.; Kitao, O.; Nakai, H.; Vreven, T.; Montgomery, J. A.; Peralta, Jr. J. E.; Ogliaro, F.; Bearpark, M.; Heyd, J. J.; Brothers, E.; Kudin, K. N.; Staroverov, V. N.; Kobayashi, R.; Normand, J.; Raghavachari, K.; Rendell, A.; Burant, J. C.; Iyengar, S. S.; Tomasi, J.; Cossi, M.; Rega, N.; Millam, J. M.; Klene, M.; Knox, J. E.; Cross, J. B.; Bakken, V.; Adamo, C.; Jaramillo, J.; Gomperts, R.; Stratmann, R. E.; Yazyev, O.; Austin, A. J.; Cammi, R.; Pomelli, C.; Ochterski, J. W.; Martin, R. L.; Morokuma, K.; Zakrzewski, V. G.; Voth, G. A.; Salvador, P.; Dannenberg, J. J.; Dapprich, S.; Daniels, A. D.; Farkas, Ö.; Foresman, J. B.; Ortiz, J. V.; Cioslowski, J.; Fox, D. J. *Gaussian 09* (Gaussian, Inc., Wallingford CT, 2009) VERSION D.01.
- [2] Adamo, C.; Barone, V., Toward reliable density functional methods without adjustable parameters: The PBE0 model. *J. Chem. Phys.* **1999**, *110*, 6158.
- [3] Dolg, M.; Wedig, U.; Stoll, H.; Preuss, H., Energy - adjusted ab initio pseudopotentials for the first row transition elements. *J. Chem. Phys.* **1987**, *86*, 866.
- [4] Andrae, D.; Haeussermann, U.; Dolg, M.; Stoll, H.; Preuss, H., Energy-adjusted ab initio pseudopotentials for the second and third row transition elements. *Theor. Chim. Acta* **1990**, *77*, 123.
- [5] Martin, J. M. L.; Sundermann, A., Correlation consistent valence basis sets for use with the Stuttgart–Dresden–Bonn relativistic effective core potentials: The atoms Ga–Kr and In–Xe. *J. Chem. Phys.* **2001**, *114*, 3408.
- [6] Jensen, J., Unifying General and Segmented Contracted Basis Sets. Segmented Polarization Consistent Basis Sets. *J. Chem. Theory Comput.*, **2014**, *10*, 1074.
- [7] te Velde, G.; Bickelhaupt, F. M.; Baerends, E. J.; Fonseca Guerra, C.; van Gisbergen, S. J. A.; Snijders, J. G.; Ziegler T., Chemistry with ADF. *J. Comp. Chem.* **2001**, *22*, 931. Amsterdam Density Functional (ADF) Theoretical Chemistry Vrieje Universitet see <http://www.scm.com/> VERSION 2014.
- [8] van Lenthe, E.; Baerends, E. J.; Snijders, J. G., Relativistic regular two-component Hamiltonians. *J. Chem. Phys.* **1993**, *99*, 4597.
- [9] van Lenthe, E.; Baerends E. J.; Snijders, J. G., Relativistic total energy using regular approximations. *J. Chem. Phys.* **1994**, *101*, 9783.
- [10] van Lenthe, E.; Baerends E. J.; Snijders, J. G., Geometry optimizations in the zero order regular approximation for relativistic effects. *J. Chem. Phys.* **1999**, *110*, 8943.
- [11] van Lenthe, E.; Baerends, E. J.; Snijders, J. G., The zero - order regular approximation for relativistic effects: The effect of spin-orbit coupling in closed shell molecules. *J. Chem. Phys.* **1996**, *105*, 6505.
- [12] van Lenthe, E.; van Leeuwen, R.; Baerends, E. J.; Snijders, J. G., Relativistic regular two-component Hamiltonians. *Int. J. Quant. Chem.* **1996**, *57*, 281.
- [13] Glendening, E. D.; Badenhoop, J. K.; Reed, A. E.; Carpenter, J. E.; Bohmann, J. A.; Morales, C. M.; Landis, C. R.; Weinhold, F.; Theoretical Chemistry Institute, University of Wisconsin, Madison, WI, USA **2013**, <http://nbo6.chem.wisc.edu/>
- [14] Bohmann, J. A.; Weinhold, F.; Farrar, T. C. J., Natural chemical shielding analysis of nuclear magnetic resonance shielding tensors from gauge-including atomic orbital calculations. *J. Chem. Phys.* **1997**, *107*, 1173.
- [15] Autschbach, J.; Zheng, T., Analyzing Pt chemical shifts calculated from relativistic density functional theory using localized orbitals: The role of Pt 5d lone pairs. *Magn. Reson. Chem.* **2008**, *46*, S45.
- [16] Autschbach, J., Analyzing NMR shielding tensors calculated with two-component relativistic methods using spin-free localized molecular orbitals. *J. Chem. Phys.* **2008**, *128*, 164112.

- [17] Aquino, F.; Pritchard, B.; Autschbach, J., Scalar Relativistic Computations and Localized Orbital Analyses of Nuclear Hyperfine Coupling and Paramagnetic NMR Chemical Shifts. *J. Chem. Theory Comput.* **2012**, *8*, 598.
- [18] a) Autschbach, J.; Zheng, S.; Schurko, R.W., Analysis of electric field gradient tensors at quadrupolar nuclei in common structural motifs. *Concepts Magn. Reson. Part A*. **2010**, *36A*, 84.
- [19] Zurek, E.; Pickard, C. J.; Autschbach, J., Density Functional Study of the ^{13}C NMR Chemical Shifts in Single-Walled Carbon Nanotubes with Stone–Wales Defects. *J. Phys. Chem. C*. **2008**, *112*, 11744.
- [20] Grimme, S.; Antony, J.; Ehrlich, S.; Krieg, H., A Consistent and Accurate ab Initio Parametrization of Density Functional Dispersion Correction (DFT-D) for the 94 Elements H-Pu. *J. Chem. Phys.* **2010**, *132*, 154104.
- [21] Marenich, A. V.; Cramer, C. J.; Truhlar, D. G., Universal Solvation Model Based on Solute Electron Density and on a Continuum Model of the Solvent Defined by the Bulk Dielectric Constant and Atomic Surface Tensions. *J. Phys. Chem. B* **2009**, *113*, 6378-6396.
- [22] O’Dell, L. A.; Schurko, R. W., QCPMG using adiabatic pulses for faster acquisition of ultra-wideline NMR spectra. *Chem. Phys. Lett.* **2008**, *464*, 97.
- [23] Perras, F. A.; Widdifield, C. M.; Bryce, D. V., QUEST Quadrupolar Exact SofTware: A fast graphical program for the exact simulation of NMR and NQR spectra for quadrupolar nuclei. *Solid State Nucl. Magn. Reson.* **2012**, *45-46*, 36.
- [24] Yamamoto, K.; Tanaka, S.; Hosoya, H.; Tsurugi, H.; Mashima, K.; Copéret, C., Activation of O_2 by Organosilicon Reagents Yields Quantitative Amounts of H_2O_2 or $(\text{Me}_3\text{Si})_2\text{O}_2$ for Efficient O-Transfer Reactions. *Helv. Chim. Acta* **2018**, doi: 10.1002/hlca.201800156
- [25] Risley, J. M.; Van Etten, R. L., Oxygen-18 isotope effect in carbon-13 nuclear magnetic resonance spectroscopy. 2. The effect of structure. *J. Am. Chem. Soc.* **1980**, *102*, 4609
- [26] Wang, W.-D.; Espenson, J. H., Pairwise Exchanges of Oxo and Imido Groups in Rhenium(VII) Compounds. *Inorg. Chem.* **2002**, *41*, 1782